

Variable X-ray Absorption toward Gravitationally-Lensed Blazar PKS 1830–211

Xinyu Dai¹, Smita Mathur¹, George Chartas², Sunita Nair³, and Gordon P. Garmire²

ABSTRACT

We present X-ray spectral analysis of five *Chandra* and *XMM-Newton* observations of the gravitationally-lensed blazar PKS 1830–211 from 2000 to 2004. We show that the X-ray absorption toward PKS 1830–211 is variable, and the variable absorption is most likely to be intrinsic with amplitudes of $\sim 2 \times 10^{22}$ – $30 \times 10^{22} \text{cm}^{-2}$ depending on whether or not the absorber is partially covering the X-ray source. Our results confirm the variable absorption observed previously, although interpreted differently, in a sequence of *ASCA* observations. This large variation in the absorption column density can be interpreted as outflows from the central engine in the polar direction, consistent with recent numerical models of inflow/outflows in AGNs. In addition, it could possibly be caused by the interaction between the blazar jet and its environment, or the variation from the geometric configuration of the jet. While the spectra can also be fitted with a variable absorption at the lens redshift, we show that this model is unlikely. We also rule out the simple microlensing interpretation of variability which was previously suggested.

Subject headings:

1. Introduction

PKS 1830–211 (Pramesh Rao & Subrahmanyan 1988; Subrahmanyan et al. 1990; Jauncey et al. 1991) consists of two $z_s = 2.507$ (Lidman et al. 1999) blazar images separated by $1''$ and lensed by a $z_l = 0.886$ (Wiklind & Combes 1996; Gerin et al. 1997) spiral galaxy

¹Department of Astronomy, The Ohio State University, Columbus, OH 43210, USA
xinyu@astronomy.ohio-state.edu, smita@astronomy.ohio-state.edu

²Department of Astronomy and Astrophysics, The Pennsylvania State University, University Park, PA 16802, USA
chartas@astro.psu.edu, garmire@astro.psu.edu

³Astronomy & Astrophysics Group, Raman Research Institute, Bangalore 560080, India, sunita@rri.res.in.

(Winn et al. 2002). PKS 1830–211 was observed in the radio (e.g., Pramesh Rao & Subrahmanyan 1988; Lovell et al. 1998), infrared (e.g., Lidman et al. 1999; Courbin et al. 2002; Winn et al. 2002), X-rays (Mathur & Nair 1997; Oshima et al. 2001; de Rosa et al. 2005; Dai et al. 2006), and Gamma-rays (Mattox et al. 1997), and the spectral energy distribution of PKS 1830–211 (de Rosa et al. 2005) shows two emission bumps with one in the infrared and the other between the hard X-ray and Gamma-ray bands.

The gravitational lens PKS 1830–211 is complicated in many aspects, and one of them is the X-ray absorption. The X-ray absorption was first detected by ROSAT (Mathur & Nair 1997). Later ASCA observations (Oshima et al. 2001) show that the X-ray absorption is variable; these authors favored a model in which microlensing was the cause of variability. Recently, PKS 1830–211 was observed by *Chandra* and *XMM-Newton* for five epochs, which enabled us to study the nature of the X-ray absorption in detail combining the angular resolution of *Chandra* and the large collecting area of *XMM-Newton*. Since the two images are resolved by *Chandra*, we can test the microlensing model predictions and study the X-ray absorption separately for the two lensed images. Dai et al. (2006) found that the differential absorption at the lens galaxy between the two images is $\Delta N_{\text{HB},A} = 1.8_{-0.6}^{+0.5} \times 10^{22} \text{ cm}^{-2}$. In this paper, we study the time evolution of the absorption in the system from the five *Chandra* and *XMM-Newton* observations and confirm that the X-ray absorption toward PKS 1830–211 is variable. Moreover, we rule out the microlensing interpretation of the observed variability.

2. Observations and Data Reduction

We observed PKS 1830–211 twice with *Chandra* and three times with *XMM-Newton* from 2000 to 2004. The details of the observations are listed in Table 1. The *Chandra* data were reduced with the CIAO3.2 software tools provided by the *Chandra* X-ray Center (CXC) following the standard threads on the CXC website.¹ Only events with standard ASCA grades of 0, 2, 3, 4, and 6 were used in the analysis. We improved the image quality of the data by removing the pixel randomization applied to the event positions by the standard pipeline. In addition, we applied a sub-pixel resolution technique (Tsunemi et al. 2001; Mori et al. 2001) to the events on the S3 chip of ACIS where the quasar images are located. This allowed us to resolve the two lensed images of the blazar. The *XMM-Newton* data were reduced using the standard analysis software SAS6.0. We used the tasks `epchain` and `emchain` from SAS to reduce the PN and MOS data, and filtered the events with patterns ≤ 4 and ≤ 12 for the PN and MOS chips, respectively.

¹The CXC website is at <http://cxc.harvard.edu/>.

3. Spectral Analysis

We fitted the spectra of PKS 1830–211 using XSPEC V11.3.1 (Arnaud 1996) in the 0.35–8 keV observed energy range for *Chandra* spectra and in the 0.35–10 keV range for *XMM-Newton* spectra. In all of our models, we fixed the Galactic absorption at $N_{\text{H}} = 0.22 \times 10^{22} \text{ cm}^{-2}$ (Dickey & Lockman 1990).

3.1. *Chandra* Spectra of Individual Images

We analyzed the *Chandra* spectra of individual images A and B. We modeled the spectra with a power law modified by the Galactic absorption and the absorption at the lens redshift; the fitting results are listed in Table 2. We experimented with two models where the power law photon indices for the two images were allowed to be different (Model 1) and where they were constrained to be the same (Model 2). We assumed that the excess absorption (above Galactic) arises in the lens galaxy at $z=0.886$ (we test this assumption later). In both the models, the column densities at the two *Chandra* epochs for image B are consistently larger than those of image A. In addition, the absorption in the first epoch is consistently larger than that in the second epoch for both images, except for image B in Model 1 where it is similar within errors. The photon indices obtained from Model 1 fits are similar for the two images and in both epochs, partially due to the large error bars on the parameter caused by the low signal-to-noise ratio of the individual spectra. The photon indices obtained from Model 2 show $\sim 1\sigma$ difference from epoch to epoch, which again is not significant. The difference between the absorption in the two images occurs simply because the lines of sight of the two images intersect different parts of the lens galaxy (Dai et al. 2006). The difference between the absorption at the two epochs indicates that the X-ray absorption is variable. The origin of the absorption variability could be either at the lens redshift or at the source redshift. We note that the differential absorption between images B and A is similar in the two epochs, especially in Model 2. This is suggestive of absorption variability occurring at the source redshift.

3.2. *Chandra* and *XMM-Newton* Spectra of Combined Images

We then analyzed the spectra of the combined images AB for the *Chandra* and *XMM-Newton* observations. We first fitted the spectra of PKS 1830–211 of the five epochs with a power-law model modified by neutral absorption from the Milky Way and the lens galaxy. The fitting results are listed in Table 3 (Model 3). We note that the absorption at the

lens redshift for this model should be treated as an averaged absorption for the two lines of sight. We also fitted the co-added three *XMM-Newton* spectra to obtain a higher signal-to-noise ratio spectrum, and the results are also listed in Table 3. The higher S/N of *XMM-Newton* spectra allows better constraints on the power-law spectral index. We find that the spectral index varies between the *Chandra* and the *XMM-Newton* observations, though variations within the *Chandra* epochs and *XMM-Newton* epochs are smaller. Comparing the fitting results of Model 3 and Model 2, the spectral index obtained by fitting the combined images AB for the *Chandra* observations are consistent with results from individual spectral fits in § 3.1. The absorption at the lens is also variable, especially when comparing the second *Chandra* observation with other epochs. We further test the variability of the spectra by comparing a model with no spectral variability (with the exception of normalization) and another model with variable absorption and spectral index. We found that the model with the spectral variability produced a better fit with a $\Delta\chi^2$ improvement of 56.1 (a null probability of 10^{-7} by the F-test) when jointly fitting the five X-ray observations. When we only consider the three *XMM-Newton* observations, the corresponding improvement is 14.5 with a null probability of 0.0097 given by the F-test. The largest absorption variation is $\Delta N_{\text{H}} = (0.7 \pm 0.3) \times 10^{22} \text{ cm}^{-2}$ between the second *Chandra* epoch and the first *XMM-Newton* epoch. Although the variable spectral index in blazars is common (e.g., Foschini et al. 2006), the absorption at the lens galaxy is unlikely to vary on the time scales of years. As discussed in § 3.1, it is more likely that the variable absorption component is at the source redshift close to the AGN, where a short time-scale variability is possible and may be expected.

The next model we tried is a power-law modified by three absorption components, the Galactic absorption and the absorptions at the lens and the source. We fixed the absorption at the lens as $N_{\text{H}} = 1.7 \times 10^{22} \text{ cm}^{-2}$, the smallest absorption column density detected in the five epochs from the previous model. This is the largest absorption column density at lens we can set to ensure no absorption variability at the lens galaxy. The fitting results are listed in Table 3 (Model 4). Again we detected variability of both the photon index and the absorption at the source redshift. Using the same test that we described in the previous model, we found that the model allowing spectral variability improved the $\Delta\chi^2$ by 59.8 with a null probability of 5×10^{-8} for jointly fitting the five X-ray observations, and an improvement of 14.7 with a null probability of 0.01 for jointly fitting the three *XMM-Newton* observations. The largest absorption variation for this model is $\Delta N_{\text{H}} = (3.5 \pm 0.7) \times 10^{22} \text{ cm}^{-2}$ between the second *Chandra* epoch and the first *XMM-Newton* epoch. The variable absorption in this model can be naturally associated with outflows from the central engine. Although, this model produces comparable fits for the two *Chandra* spectra compared with Model 3, where there is no absorption at the source redshift, the fits for the *XMM-Newton* spectra with a higher S/N are worse than Model 3 with $\Delta\chi^2$ increases of 5.8, 37.2, 13.0 for the

three *XMM-Newton* spectra. We also tested whether fitting the absorption component at the source with a warm absorber or a partially covering absorber would improve the fit. While the warm absorber model produces a worse fit, the partial covering model (Table 3, Model 5) produces comparable fits to Model 3. For the partial covering model, the model allowing spectral variability produces improvement of the $\Delta\chi^2$ by 79.7 with a null probability of 1×10^{-11} for jointly fitting the five X-ray observations, and an improvement of 14.1 with a null probability of 0.01 for jointly fitting the three *XMM-Newton* observations. The largest absorption variation for this model is $\Delta N_{\text{H}} = (29 \pm 7) \times 10^{22} \text{ cm}^{-2}$, again, between the second *Chandra* epoch and the first *XMM-Newton* epoch.

As a final improvement to our model, we assume that the lines of sight of the two lensed images pass through different locations in the lens galaxy and thus have different absorption column densities. This differential absorption is measured as $\Delta N_{\text{H},A} = 1.8_{-0.6}^{+0.5} \times 10^{22} \text{ cm}^{-2}$ (Dai et al. 2006). Therefore, we have a model composed of two power-law components and each of them is modified by three absorptions from Galactic, lens, and source. The two power-law components representing the two lensed images have the same photon index but different normalizations. The normalization ratio between images A and B is constrained as $R = 1.03$ by taking the hard X-ray flux ratios (3–8 keV) from the *Chandra* observation. The Galactic absorption and the absorption at the source are the same for the two power-law components, and the absorbers at the source are assumed to be partially covering the continuum. The absorber column densities at the lens are different for the two power-law components by the amount given by Dai et al. (2006). We fit the two *Chandra* spectra and the co-added *XMM-Newton* spectrum simultaneously with this model. We constrained that the absorption at lens did not vary. The fitting results are listed in Table 3 (Model 6), and the spectra are shown in Figure 1. The fitting results indicate that the absorption at the source has varied by roughly $(39 \pm 7) \times 10^{22} \text{ cm}^{-2}$.

4. Discussion

We detected the variable absorption, variable power-law photon index, and variable flux for the blazar PKS 1830–211. The observed variability between *Chandra* and *XMM-Newton* spectra could be, in part, due to imperfect cross-calibration between the two. However for high S/N spectra, the cross-calibration between *Chandra* and *XMM-Newton* can yield a spectral difference of $\Delta\Gamma \sim 0.03^2$, whereas our measured differences are between $\Delta\Gamma \sim 0.15$ – 0.3 . In addition, the higher S/N *XMM-Newton* spectra show a statistically significant

²http://xmm.esac.esa.int/external/xmm_sw_cal/calib/cross_cal/index.php

variability within the three *XMM-Newton* observations ($\Delta\chi^2$ improvement of 14.5, 14.7, and 14.1 for Models 3, 4, and 5 with spectral variability). We also found the spectral variability between the two *Chandra* observations, where the second *Chandra* epoch has consistently lower absorption column densities than the first observation. This is better demonstrated in § 3.1, where we analyzed the individual spectra of each image. We plot the variations of absorption in Figure 2, photon index variations in Figure 3, and the photon index against unabsorbed flux in Figure 4. It is well known that blazars are variable, so the observed spectral variability is not surprising in itself. We also found that the photon index and flux are correlated (Figure 4). This relation has been observed in several Gamma-ray loud AGNs (Foschini et al. 2006). PKS 1830–211 provides an additional example of a source following this correlation.

The variable absorption is more intriguing. The variable absorption toward PKS 1830–211 was detected previously with *ASCA* observations (Oshima et al. 2001), although interpreted differently. Oshima et al. (2001) obtained a variation amplitude of $\sim 0.5 \times 10^{22} \text{cm}^{-2}$ when modeling the absorption at the lens, which is consistent with our measurement of $\sim 0.6 \times 10^{22} \text{cm}^{-2}$ (Model 3). We note that the variation detected by Oshima et al. (2001) is on the timescale of 10 days while that found by us is on the timescale of years. It is possible that the variable absorption is at the source redshift. Depending on the nature of the absorber, we obtained variations of $\sim 2 \times 10^{22} \text{cm}^{-2}$ and $\sim 30 \times 10^{22} \text{cm}^{-2}$ for a fully covering absorber (Model 4) and a partially covering absorber (Model 5, 6), respectively. The other possibilities are microlensing models.

Oshima et al. (2001) proposed a microlensing interpretation to explain the apparent variable absorption. The basic idea is that the absorption does not vary but is different for the two images, and the microlensing produces flux changes between the two images which appears as variable absorption. As we discussed in the spectral fits to individual *Chandra* images (§ 3.1), the absorption varies in individual images between the two epochs, which cannot be attributed to this simple microlensing model. For this reason, we rule out the simple microlensing model as the cause of variable absorption in PKS 1830–211. More complicated microlensing models are required which must involve significant emission size differences between the soft and hard X-ray regions to interpret the data. However, even these models will have difficulty explaining the similar differential absorptions between images A and B for the two *Chandra* epochs. Microlensing will only produce uncorrelated changes between the images.

Variable absorption thus appears to be a robust result, independent of model. The variability can either come from the lens or from the source redshift. If the variable absorption is at the lens, a variability amplitude of $\sim 0.6 \times 10^{22} \text{cm}^{-2}$ can sufficiently parameterize the

Chandra and *XMM-Newton* spectra without invoking any absorption at the source. Recently, variable Mg II absorption has been detected in an intervening absorber in front of a Gamma-ray burst (Hao et al. 2006). The observed Mg II column density changes as the burst expands geometrically (Frank et al. 2006). Similarly, if the size of the blazar changes with luminosity, it may produce variable absorption at the lens. Another mechanism that can produce variable absorption at the lens galaxy is proposed by Dong (2006), where microlensed images, slightly shifted from the original image position, intersect slightly different positions at the lens, producing variable absorption. However, in PKS 1830–211, the differential absorption of the two images in the two *Chandra* epochs is similar, arguing against the variability at the lens. It is far more likely that the variable absorption is intrinsic to the blazar, simply because there are other AGNs with variable intrinsic absorption, including blazars (see below).

While the absorption toward the gravitational lens PKS 1830–211 is very complicated, with the sequence of *Chandra* and *XMM-Newton* observations, a converging picture is emerging. Besides the Galactic absorption of $N_{\text{H}} = 22.27 \times 10^{20} \text{ cm}^{-2}$ (Dickey & Lockman 1990), there is also an intrinsic absorption and absorption from the lens galaxy. The absorption column densities in the lens galaxy are different for the two lensed images by $\Delta N_{\text{H},A} = 1.8_{-0.6}^{+0.5} \times 10^{22} \text{ cm}^{-2}$ (Dai et al. 2006), and this is consistent with the differential extinction measurement between the two images and a Galactic dust-to-gas ratio. The amplitude of the variability of the intrinsic absorption is model dependent with amplitudes of $\sim 2 \times 10^{22} - 30 \times 10^{22} \text{ cm}^{-2}$.

Recently, the intrinsic absorption for blazars has been reported in several cases, such as GB B1428+4217 (Worsley et al. 2004a), PMN J0525–3343 (Worsley et al. 2004b), and RBS 315 (Piconcelli & Guainazzi 2005; see also Tavecchio et al. 2007). In this paper, we present variable intrinsic absorption toward gravitationally-lensed blazar PKS 1830–211. The large variation in the absorption column density can be interpreted as outflows similar to those detected in BAL QSOs. However, as PKS 1830–211 is a blazar, this outflow must be in the polar direction. Recent numerical simulations of accretion flows in AGNs (Proga 2006) discussed the cases of polar outflows; our observations of PKS 1830–211 might be providing an example in support of such models. In addition, it is also possible that the intrinsic absorption variation is caused by the interaction between the blazar jet and its environment, or the variation from the geometric configuration of the jet. More intense monitoring of this system or further variability studies using a large sample of blazars are needed to better constrain the nature of their X-ray spectral variation.

REFERENCES

- Arnaud, K. A. 1996, ASP Conf. Ser. 101: Astronomical Data Analysis Software and Systems V, ed. Jacoby G. & Barnes J., 17
- Courbin, F., Meylan, G., Kneib, J.-P., & Lidman, C. 2002, ApJ, 575, 95
- Dai, X., Kochanek, C. S., Chartas, G., & Mathur, S. 2006, ApJ, 637, 53
- Dong, Subo 2006, ApJ submitted, astro-ph/0612403
- de Rosa, A., Piro, L., Tramacere, A., Massaro, E., Walter, R., Bassani, L., Malizia, A., Bird, A. J., & Dean, A. J. 2005, A&A, 438, 121
- Dickey, J. M. & Lockman F. J. 1990, ARA&A 28, 215
- Frank, S., et al. 2006, ApJ submitted, astro-ph/0605676
- Foschini, L., et al. 2006, astro-ph/0603268
- Garmire, G. P., Bautz, M. W., Nousek, J. A., & Ricker, G. R. 2003, SPIE, 4851, 28
- Gerin, M., Phillips, T. G., Benford, D. J., Young, K. H., Menten, K. M., & Frye, B. 1997, ApJ, 488, L31
- Hao, H., Stanek, K. Z., Dobrzycki, A., Matheson, T., Bentz, M. C., Kuraszkiewicz, J., Garnavich, P. M., Howk, J. C., Calkins, M. L., Worthey, G., Modjaz, M., & Serven J. 2006, ApJ Letter submitted, astro-ph/0612409
- Jauncey, D. L., et al. 1991, Nature, 352, 132
- Lidman, C., Courbin, F., Meylan, G., Broadhurst, T., Frye, B., & Welch, W. J. W. 1999, ApJ, 514, L57
- Lovell, J. E. J., Jauncey, D. L., Reynolds, J. E., Wieringa, M. H., King, E. A., Tzioumis, A. K., McCulloch, P. M., & Edwards, P. G. 1998, ApJ, 508, L51
- Mathur, Smita & Nair, Sunita 1997, ApJ, 484, 140
- Mattox, J. R., Schachter, J., Molnar, L., Hartman, R. C., & Patnaik, A. R. 1997, ApJ, 481, 95
- Mori, K., Tsunemi, H., Miyata, E., Baluta, C., Burrows, D. N., Garmire, G. P., & Chartas, G. 2001, in ASP Conf. Ser. 251, New Century of X-Ray Astronomy, ed. H. Inoue & H. Kunieda (San Francisco: ASP), 576

- Oshima, T., Mitsuda, K., Ota, N., Yonehara, A., Hattori, M., Mihara, T., & Sekimoto, Y. 2001, *ApJ*, 551, 929
- Piconcelli, E., & Guainazzi, M. 2005, *A&A*, 442, L53
- Pramesh Rao, A., & Subrahmanyan, R. 1988, *MNRAS*, 231, 229
- Proga, Daniel 2006, astro-ph/0610383
- Subrahmanyan, R., Narasimha, D., Pramesh-Rao, A., & Swarup, G. 1990, *MNRAS*, 246, 263
- Tavecchio, F., Maraschi, L., Ghisellini, G., Kataoka, J., Foschini, L., Sambruna, R. M., & Tagliaferri, G. 2007, *ApJ*, 665, 980
- Tsunemi, H., Mori, K., Miyata, E., Baluta, C., Burrows, D. N., Garmire, G. P., & Chartas, G. 2001, *ApJ*, 554, 496
- Weisskopf, M. C., Brinkman, B., Canizares, C., Garmire, G., Murray, S., & Van Speybroeck, L. P. 2002, *PASP*, 114, 1
- Wiklind, T. & Combes, F. 1996, *Nature*, 379, 139
- Winn, Joshua N., Kochanek, Christopher S., McLeod, Brian A., Falco, Emilio E., Impey, Christopher D., & Rix, Hans-Walter 2002, *ApJ*, 575, 103
- Worsley, M. A., Fabian, A. C., Celotti, A., & Iwasawa, K. 2004a, *MNRAS*, 350, L67
- Worsley, M. A., Fabian, A. C., Turner, A. K., Celotti, A., & Iwasawa, K. 2004b, *MNRAS*, 350, 207

Table 1. List of X-Ray Observations of PKS 1830–211

Date	Telescope	Grating?	Exposure Time (sec)
2000-06-26	<i>Chandra</i>	HETGS	47471
2001-06-25	<i>Chandra</i>	HETGS	51219
2004-03-10	<i>XMM-Newton</i>	none	8328
2004-03-24	<i>XMM-Newton</i>	none	27004
2004-05-05	<i>XMM-Newton</i>	none	21356

Table 2. Spectral Analysis for Individual *Chandra* Spectra of PKS 1830–211.

Date	Image	$N_{\text{H}}(z=0.886)$, 10^{22} cm^{-2}	Γ	$\chi^2(dof)$
Model 1: An absorbed power-law				
2000-06-26	A	1.6 ± 0.4	1.09 ± 0.09	100.5(108)
2000-06-26	B	3.5 ± 1.1	1.13 ± 0.15	129.6(106)
2001-06-25	A	0.8 ± 0.5	0.96 ± 0.09	140.7(120)
2001-06-25	B	3.3 ± 1.0	1.11 ± 0.12	113.8(116)
Model 2: An absorbed power-law with $\Gamma_A = \Gamma_B$.				
2000-06-26	A	1.6 ± 0.4	1.10 ± 0.07	229.6(215)
2000-06-26	B	3.4 ± 0.7
2001-06-25	A	1.0 ± 0.4	1.02 ± 0.06	255.2(237)
2001-06-25	B	2.8 ± 0.6

Note. — Galactic N_{H} is fixed at $N_{\text{H}} = 22.27 \times 10^{20} \text{ cm}^{-2}$ (Dickey & Lockman 1990) for all models.

Table 3. Spectral Analysis of Combined Images of PKS 1830–211.

Parameters	<i>Chandra</i>		<i>XMM-Newton</i>			XMM-Co-Added
	I	II	I	II	III	
Date	2000-06-26	2001-06-25	2004-03-10	2004-03-24	2004-05-05	...
Model 3: A power-law with absorption at the lens and the Galaxy						
$N_{\text{H}}(z = 0.89, 10^{22} \text{ cm}^{-2})$	2.27 ± 0.26	1.70 ± 0.22	2.42 ± 0.12	2.37 ± 0.07	2.29 ± 0.07	2.34 ± 0.04
Γ	1.07 ± 0.05	0.99 ± 0.04	1.18 ± 0.02	1.14 ± 0.01	1.17 ± 0.01	1.16 ± 0.01
Unabsorbed Flux ^a	0.92 ± 0.02	0.97 ± 0.03	1.50 ± 0.03	1.42 ± 0.02	1.28 ± 0.02	1.38 ± 0.01
$\chi^2(dof)$	365.6(305)	365.6(337)	151.8(152)	447.3(396)	314.3(301)	843.7(743)
Model 4: Same as Model 3, with additional absorption at the source ^b						
$N_{\text{H}}(z = 2.51, 10^{22} \text{ cm}^{-2})$	$1.24^{+1.10}_{-1.19}$	< 0.38	3.47 ± 0.60	2.80 ± 0.33	2.68 ± 0.36	2.80 ± 0.22
Γ	1.02 ± 0.05	0.99 ± 0.03	1.17 ± 0.02	1.12 ± 0.01	1.16 ± 0.01	1.14 ± 0.01
Unabsorbed Flux	0.91 ± 0.04	0.97 ± 0.03	1.50 ± 0.03	1.41 ± 0.02	1.28 ± 0.02	1.38 ± 0.01
$\chi^2(dof)$	369.9(305)	365.6(337)	157.6(152)	484.5(396)	327.3(301)	899.3(743)
Model 5: Same as Model 4, but with a partially covering absorber at the source ^b						
$N_{\text{H}}(z = 2.51, 10^{22} \text{ cm}^{-2})$	< 4.6	< 0.7	$29.0^{+8.0}_{-4.8}$	$24.2^{+4.3}_{-2.8}$	$19.5^{+6.1}_{-3.8}$	25.0 ± 2.5
Covering Factor	0.44 (fixed)	0.44 (fixed)	0.50 ± 0.05	0.43 ± 0.03	0.40 ± 0.04	0.44 ± 0.02
Γ	1.00 ± 0.04	0.98 ± 0.03	1.32 ± 0.05	1.23 ± 0.03	1.23 ± 0.03	1.26 ± 0.02
Unabsorbed Flux	0.91 ± 0.04	0.97 ± 0.04	1.70 ± 0.06	1.53 ± 0.04	1.36 ± 0.04	1.51 ± 0.03
$\chi^2(dof)$	370.6(305)	365.9(337)	137.4(151)	447.4(395)	315.6(300)	827.0(742)
Model 6: Same as Model 5, but with two different power-law components ^c						
$N_{\text{H}A} (z = 0.89, 10^{22} \text{ cm}^{-2})$				1.57 ± 0.07		
$N_{\text{H}}(z = 2.51, 10^{22} \text{ cm}^{-2})$	< 1.7	< 0.7	39 ± 7
Covering Factor				0.23 ± 0.04		
Γ	1.07 ± 0.03	1.07 ± 0.02	1.27 ± 0.03
$\chi^2(dof)$				1488.8(1367)		

Note. — Galactic N_{H} is fixed at $N_{\text{H}} = 22.27 \times 10^{20} \text{ cm}^{-2}$ (Dickey & Lockman 1990) for all models.

^aThe unabsorbed fluxes in all models are calculated between 0.4–8 keV and in units of $10^{-12} \text{ erg cm}^{-2} \text{ s}^{-1}$.

^bThe absorption at lens is fixed at $N_{\text{H}} = 1.7 \times 10^{22} \text{ cm}^{-2}$ for this model.

^dThe absorption of the lens galaxy for image B is constrained as $N_{\text{H}B} = N_{\text{H}A} + 1.8 \times 10^{22} \text{ cm}^{-2}$.

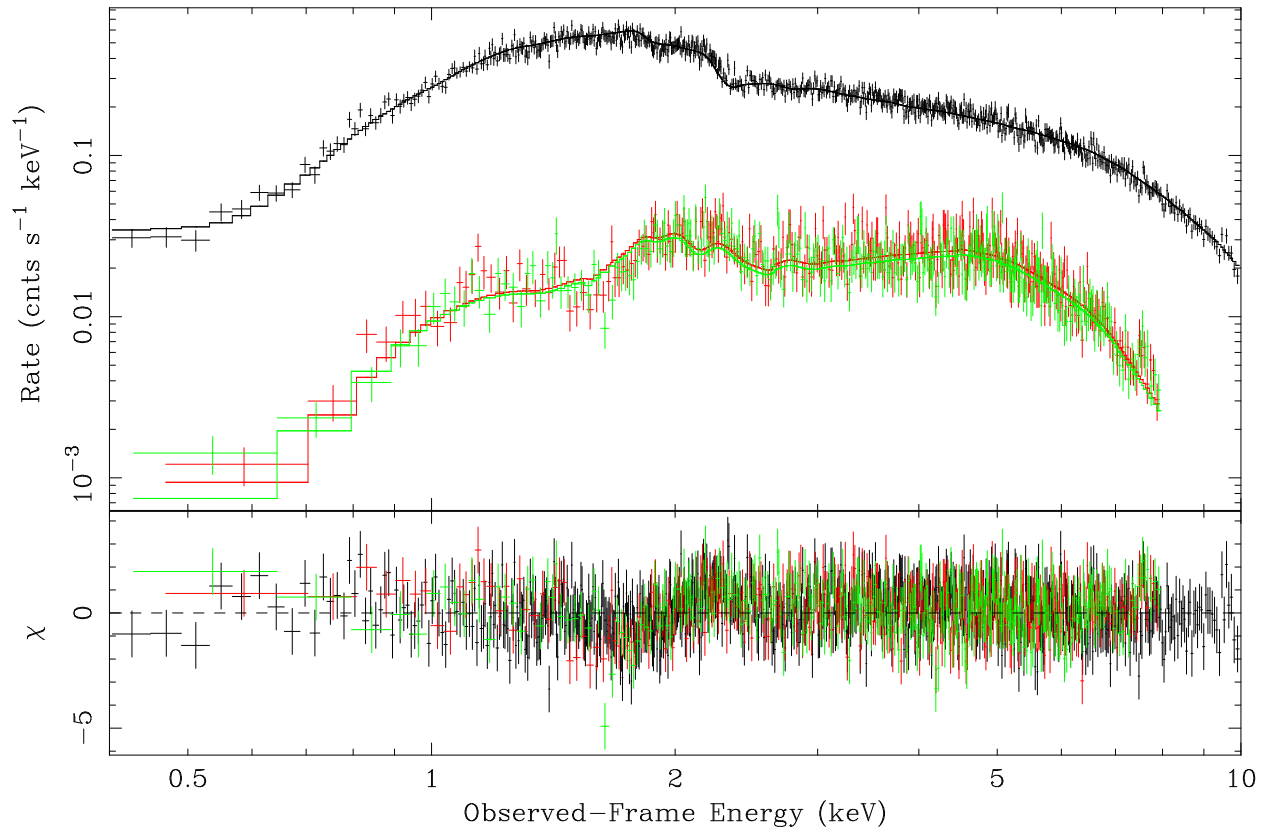


Fig. 1.— *XMM-Newton* and *Chandra* spectra of PKS 1830–211. The top spectrum is a combined spectrum from three *XMM-Newton* observations, and the bottom two spectrum is from the two *Chandra* observations. The spectra are fitted simultaneously with absorbed power-law models as described in Model 6 of Table 3.

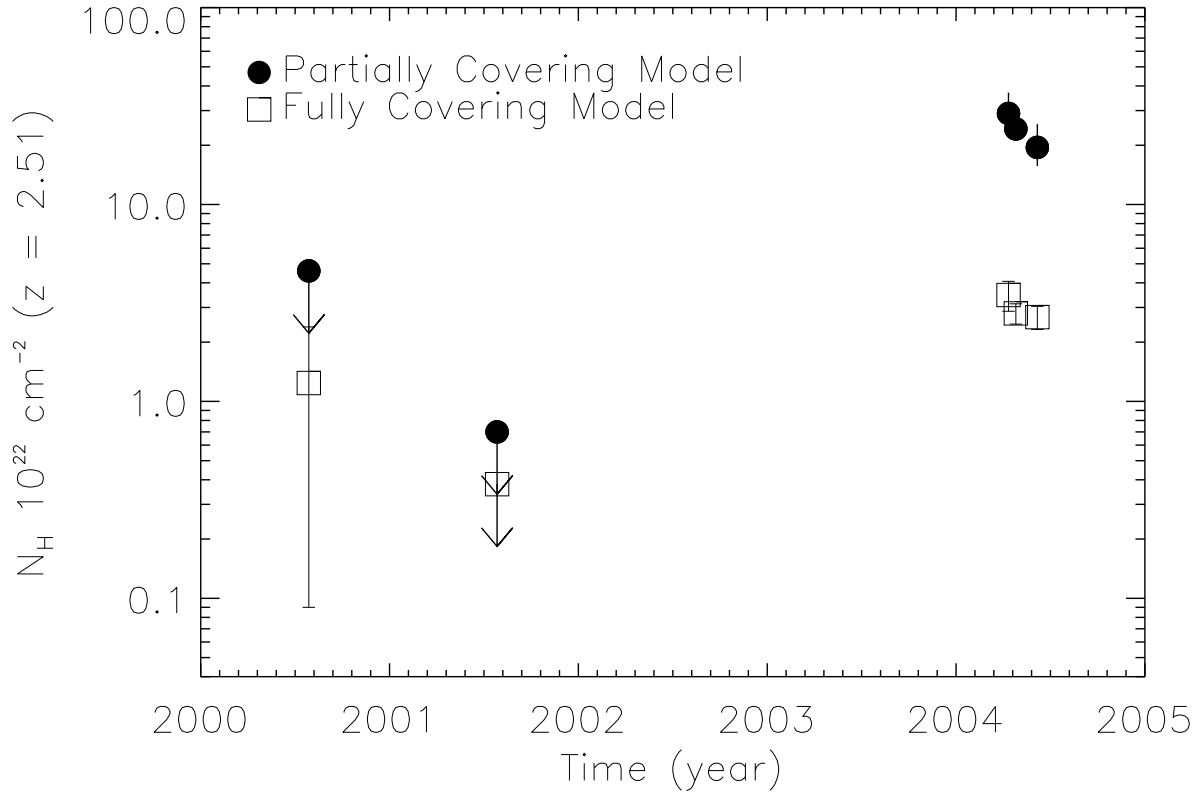


Fig. 2.— The absorption column densities at the redshift of the source ($z = 2.51$) of PKS 1830–211 measured from *Chandra* and *XMM-Newton* spectra assuming a partial covering model (filled circles) and a fully covering absorption model (squares).

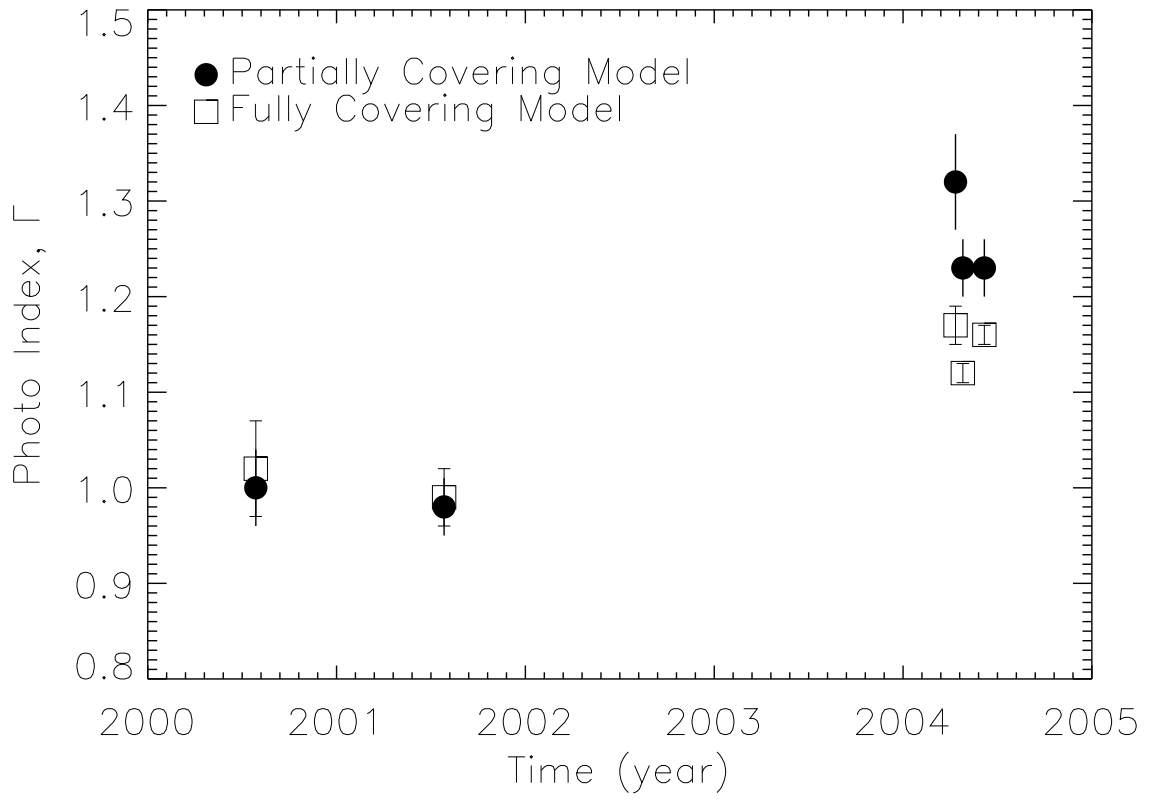


Fig. 3.— The photon indices measured for PKS 1830–211 from *Chandra* and *XMM-Newton* observations.

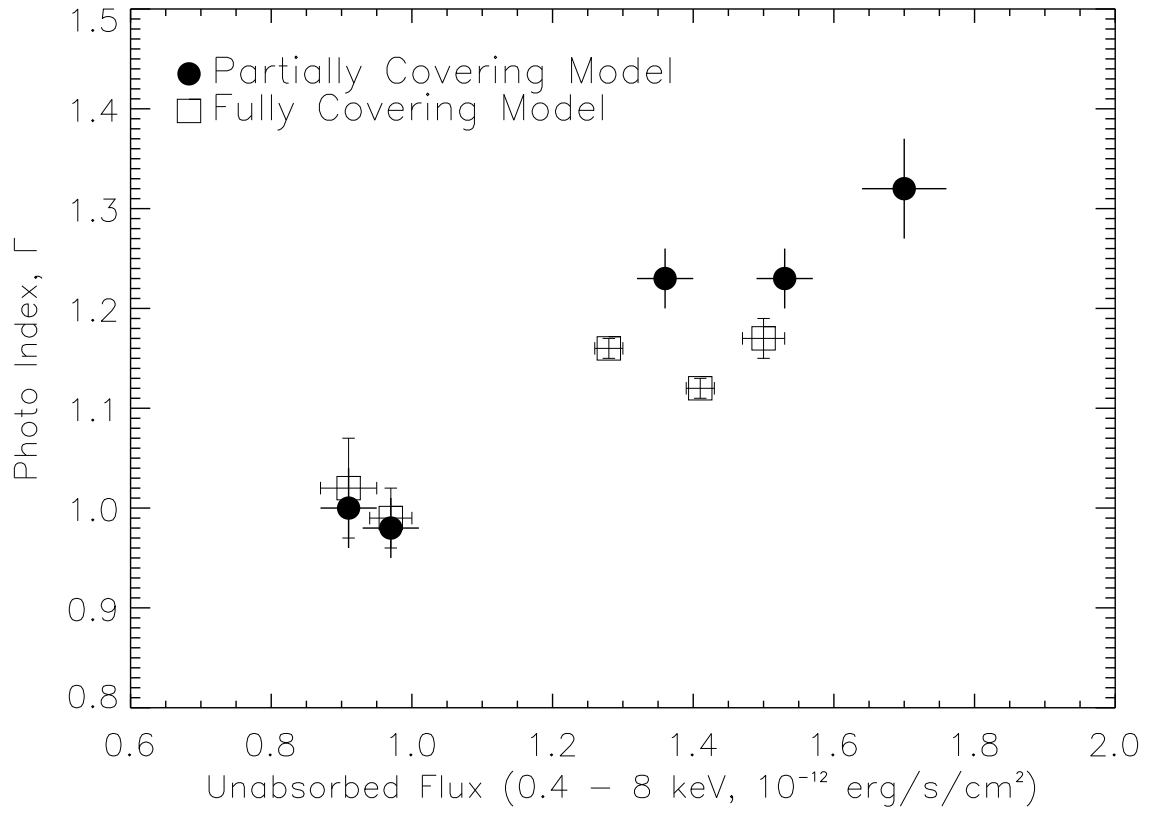


Fig. 4.— The photon indices versus flux for PKS 1830–211 from *Chandra* and *XMM-Newton* observations.